Hartree-Fock phase diagram of the two-dimensional electron gas

B. Bernu,[1] F. Delyon,[2] M. Holzmann,[1,3] and L. Baguet[1]
[1]*LPTMC, UMR 7600, CNRS, Université Pierre et Marie Curie, Paris, France*
[2]*CPHT, UMR 7644, CNRS, École Polytechnique, Palaiseau, France*
[3]*Université Grenoble 1/CNRS, LPMMC UMR 5493, Maison des Magistères, F-38042 Grenoble, France*
(Received 17 June 2011; revised manuscript received 2 August 2011; published 15 September 2011)

We calculate the ground-state phase diagram of the homogeneous electron gas in two dimensions within the Hartree-Fock approximation. At high density, we find stable solutions, where the electronic charge and spin density form an incommensurate crystal having more crystal sites than electrons, whereas the commensurate Wigner crystal is favored at lower densities, $r_s \gtrsim 1.22$. Our explicit calculations demonstrate that the homogeneous Fermi-liquid state, though being an exact stationary solution of the Hartree-Fock equations, is never the Hartree-Fock ground state of the electron gas.

DOI: 10.1103/PhysRevB.84.115115 PACS number(s): 71.10.Ca, 71.10.Hf, 71.30.+h

I. INTRODUCTION

Electrons are found everywhere in matter, most of the time localized by positive charges. In typical condensed-matter situations, electronic densities and temperatures are such that, in addition to the external positive charges, a quantum description of electrons interacting with each other is necessary, leading, in general, to a difficult quantum many-body problem. The homogeneous electron gas, where the positive charges are reduced to solely ensure global electroneutrality, is one of the most fundamental models to study electronic correlation effects. In three dimensions, $d = 3$, valence electrons in alkaline metals realize the electron gas to high precision, in particular in solid sodium,[1] whereas the two-dimensional electron gas (2DEG), $d = 2$, and its extension to quasi two dimensions[2] is relevant for electrons at heterostructures, e.g., semiconductor-insulator interfaces.[3] At zero temperature, the electron gas is described by a single parameter, the density n, or, equivalently, by the dimensionless parameter $r_s = a/a_B$. Here $a = [2(d-1)\pi n/d]^{-1/d}$ is the mean interparticle distance, and $a_B = \hbar^2/(me^2)$ is the Bohr radius, where $-e$ and m are the electronic charge and mass, respectively.

As pointed out by Wigner,[4] at low densities and zero temperature, electrons will form a crystal, which is supposed to melt at higher densities where the kinetic energy dominates over the interaction. In the limit $r_s \to 0$, the Hartree-Fock approximation (HF) applies. Since the noninteracting Fermi sea remains a stationary solution of the Hartree-Fock equations, it is natural to assume a Fermi-liquid phase at high densities. First-principles calculations, such as quantum Monte Carlo,[5–8] have located the transition from the Wigner crystal (WC) to the homogeneous Fermi liquid (FL) to high precision. Still, there are indications that the Fermi-liquid phase is not necessarily the absolute ground state of the electron gas at high densities[9–11,16] and that a direct transition between Wigner crystal and a homogeneous Fermi liquid cannot occur in two dimensions in the thermodynamic limit.[12–14] These conjectures actually hold already for the electron gas in the Hartree-Fock approximation, but despite the early predictions by Overhauser of the spin and charge density instability of the Fermi-liquid ground state, explicit, numerical HF calculations[15] have not confirmed them for a long time. Based on Bloch functions, these HF calculations[15] studied unpolarized and polarized Wigner-crystal phases of square and triangular symmetries and found a first-order transition to the unpolarized Fermi gas that, within this study, remains the lowest-energy state for $r_s \lesssim 1.44$. Only recently, the first self-consistent Hartree-Fock solutions with energies below the Fermi-liquid energy have been found at high densities.[11]

The HF solutions of Ref. 11 obtained without imposing any periodicity in the density show that the fully polarized electron gas in two dimensions forms a periodic charge density with triangular symmetry at high densities. In contrast to the low-density Wigner crystal, the number of maxima of the charge density is higher than the number of electrons, having thus metallic character, and we will refer to such states as incommensurate crystals in the following. However, incommensurate states give rise to important size effects, and the calculations in Ref. 11 were limited to ∼500 electrons.

In this paper, we extend the description based on Bloch waves to study arbitrary modulation and occupation number. We focus on the density region $r_s < 4$, where incommensurate states may occur. We show how the incommensurate states can be represented by the vector Q of the charge modulation. Restricting the search for the HF ground state to states with arbitrary Q, we are able to overcome size restrictions, and we explore the phase diagram of the 2DEG including triangular and square symmetries. While our minimization also includes the possibility of partial polarized states, they do not occur as ground states, which are either unpolarized (U) or fully polarized (P); in particular, we show that the incommensurate unpolarized crystal is favored at high densities. Whereas the momentum distribution of the Wigner crystal is a continuous function of the momentum, we show that there are angle-selective steps in the incommensurate phase.

II. METHODS

The Hamiltonian of the electron gas containing N electrons reads

$$H = -\frac{1}{2}\sum_i \Delta_i + \sum_{1\leqslant i<j\leqslant N_p} v(x_i - x_j), \qquad (1)$$

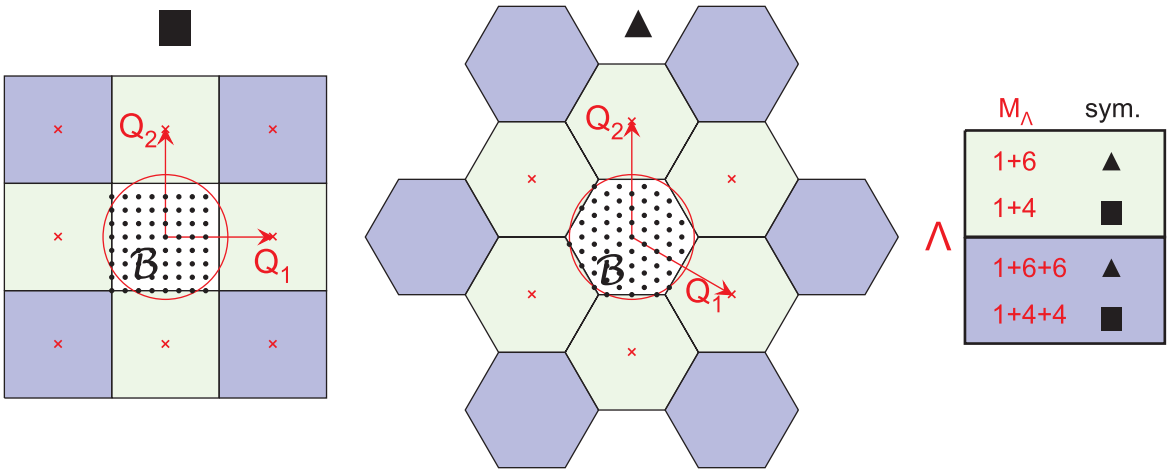

FIG. 1. (Color online) Illustration of the k space in the (left) square and (right) triangular geometry. At the center of each graph are shown the Brillouin zone $\mathcal{B}$ (in white) and the corresponding basis vectors Q_1 and Q_2. The first and second shells of neighboring cells, $\mathcal{B}+n_1Q_1+n_2Q_2$, are shaded in light green and light blue, respectively. For square (triangular) symmetry, the integers n_i of the first and second shells satisfy $n_1^2+n_2^2=1,2$ ($n_1^2+n_2^2-n_1n_2=1,3$). The corresponding number of cells is summarized by M_Λ in the right column. Most of the results presented in this paper are done including a number of bands M_Λ, which corresponds to two neighboring shells for the square and one for the triangular geometry. In light red, we indicate the elementary cell $\mathcal{B}_0$ used in our numerical calculations; the $N_\mathcal{B}$ black dots are an example of the discretization of the Brillouin zone (here $N_\mathcal{B}=M^2$ with $M=8$, as explained in Sec. III). The circle indicates the Fermi surface of a Fermi gas.

where Δ_i is the Laplacian with respect to x_i, $v(x)$ is the electrostatic interaction $v(x)=\|x\|^{-1}$, and we have used atomic units where distances are measured in units of a_B and energies in Hartree, $1\text{Ha}=\hbar^2/(ma_B^2)$. In addition to Eq. (1), the interaction between electrons and a positive background charge must be considered to ensure charge neutrality.

We are considering N electrons in a finite box of volume V, of sizes L_1 and L_2, with periodic boundary conditions, so that the momentum k belongs to the lattice L^* generated by L_1^* and L_2^* satisfying $L_iL_j^*=2\pi\delta_{ij}$.

Within the Hartree-Fock approximation, the energy expectation value is minimized with respect to a single skew-symmetric product of N single particle states. Periodic solutions are special states, which can be described by Bloch waves. Let Λ be a sublattice of L^* generated by Q_1 and Q_2. The Brillouin zone is defined as the Voronoi cell of the origin, and a periodic state is given by $|\varphi_k\rangle=\sum_{q\in\Lambda}a_k(q)|k+q\rangle$, where k belongs to the Brillouin zone $\mathcal{B}$ (see Fig. 1).

As a particular case, the WC is obtained by choosing Λ such that the Brillouin zone $\mathcal{B}$ contains exactly N states, where N is the number of electrons. Thereafter, the state is built as $\wedge_{k\in\mathcal{B}}|\varphi_k\rangle$. An upper bound of the ground-state energy is obtained by minimizing the coefficients $a_k(q)$ of the Bloch functions. As r_s approaches zero, the kinetic energy dominates,

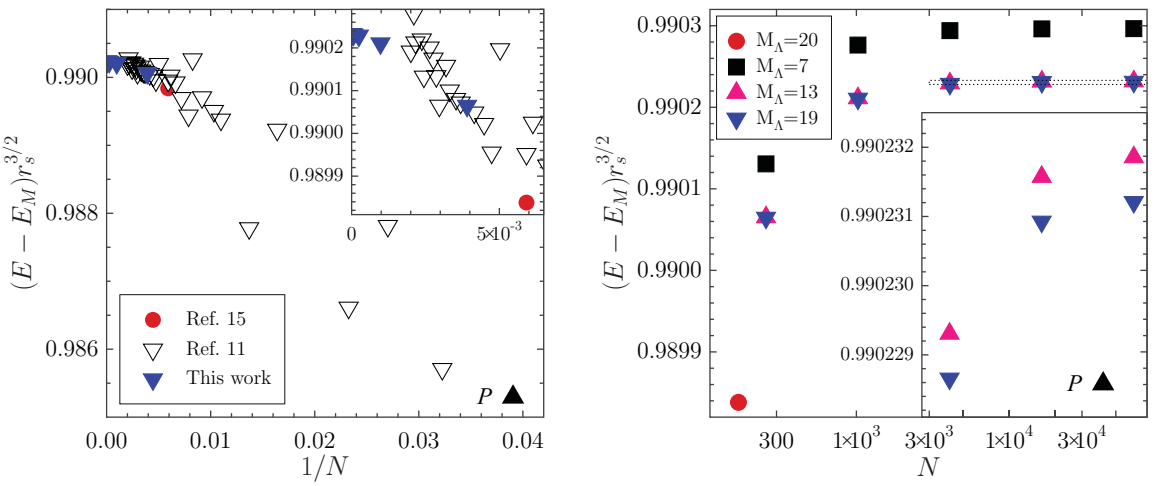

FIG. 2. (Color online) Energy (in Hartree units) of the 2DEG in the triangular symmetry at $r_s=4$ (WC) as a function of the number of particles, $N\equiv N_\mathcal{B}$, and the number of included bands M_Λ. $E_M=-1.1061/r_s$ is the Madelung energy. (**P**▲ indicates polarized final state with triangular geometry.) (left) Comparison with previous work.[11,15,17] Blue solid downward triangles are the results of the present work using $M_\Lambda=19$. (right) Convergence with respect to N and M_Λ. The inset is a zoom of the dotted-line domain.

which is minimized by the Fermi gas (FG) defined by $k \leqslant k_F$ (see below). Such a state cannot be described by the WC. In Ref. 11, the HF energy of the polarized gas has been minimized without imposing periodicity of the solutions; nevertheless, at intermediate densities, the HF ground states are periodic with larger modulations than in the WC corresponding to less electrons than states in the Brillouin zone.

In this paper we focus on periodic solutions with arbitrary modulations. For a given modulation and for fixed choice of k vectors in the Brillouin zone the energy computation is fast enough to tackle millions of electrons as every single state is described by very few parameters only. However, the minimization with respect to the choice of k vectors in the Brillouin zone becomes a complicated combinatorial problem. This combinatory problem is simplified within the framework of density matrix.

The one-body density matrix ρ_1 is a symmetric positive matrix such that $\mathrm{Tr}\rho_1 = 1$. Provided that $\rho_1 \leqslant 1/N$, this matrix can be seen as a one-body density matrix of a state of N electrons. In the thermodynamic limit, the two-body uncorrelated density matrix can be expressed in terms of ρ_1 as

$$\rho_2(1,2;1',2') = \rho_1(1;1')\rho_1(2;2') - \rho_1(1;2')\rho_1(2;1'). \quad (2)$$

The total energy, *a priori* a function of the reduced one and two-body density matrices, can be expressed entirely as a functional of ρ_1. Explicitly, we obtain for the energy per particle in atomic units:

$$E = \frac{1}{2}\sum_{k\in L^*,\sigma} k^2\rho_1(k,\sigma;k,\sigma) + \sum_{\substack{q,k_1,k_2\in L^* \\ \sigma_1,\sigma_2}} \frac{v_q}{r_s^2}\rho_2(k_1,\sigma_1,k_2,\sigma_2;k_1+q,\sigma_1,k_2-q,\sigma_2) \quad (3)$$

where $v_q = 1/\|q\|$ for $q \neq 0$ and $v_0 = 0$. For instance, the unpolarized Fermi gas (UFG) corresponds to $\rho_1(k\sigma,k'\sigma') = \delta_{kk'}\delta_{\sigma\sigma'}\Theta(k_{F,U} - \|k\|)/N$ with $\pi k_{F,U}^2 = 2\pi^2 N/V$; the resulting energy is $E_{FG}^U = 1/(2r_s^2) - 8/(3\pi\sqrt{2}r_s)$, and the fully polarized Fermi gas (PFG) corresponds to $\rho_1(k\sigma,k'\sigma') = \delta_{kk'}\delta_{\sigma+}\delta_{\sigma\sigma'}\Theta(k_{F,P} - \|k\|)/N$, with $\pi k_{F,P}^2 = (2\pi)^2 N/V$ and energy $E_{FG}^P = 1/r_s^2 - 8/(3\pi r_s)$. In general, without any specification, k_F denotes the Fermi wave vector according to the polarization of the corresponding state.

In the following we restrict the density matrix to represent periodic solutions. The corresponding one-body density matrix can be written as

$$\rho_1(1,1') \equiv \rho_1(k+q,\sigma;k+q',\sigma') \equiv \rho_k(q,\sigma;q',\sigma'), \quad (4)$$

with $q,q' \in \Lambda$ and k in the Brillouin zone $\mathcal{B}$. Thus, the density matrix is now described by a family of positive matrices ρ_k such that $\rho_k \leqslant 1/N$ and $\sum_k \mathrm{Tr}\rho_k = 1$.

Numerically, we truncate the number of lattice vectors of the sublattice Λ and include only the first M_Λ vectors of smallest norm in the numerical calculations. In the framework of band structure calculations, where the Bloch states are obtained from an external periodic potential, M_Λ corresponds to the number of bands considered. Thus ρ_k is a $2M_\Lambda \times 2M_\Lambda$ matrix and in order to fulfill the condition $\rho_k \leqslant 1/N$, it is more convenient to write

$$\rho_k = U_k^* D_k U_k, \quad (5)$$

where D_k is a diagonal matrix with $0 \leqslant D_k \leqslant 1/N$ and U_k is a unitary matrix. The potential energy contains a convolution in momentum space calculated using fast Fourier transform (FFT). The minimization of the HF energy is done computing the gradient of the energy with respect to U_k and D_k. The only drawback of the method is to fulfill the condition $D_k \leqslant 1/N$.

The minimization at a given density consists of the following steps. At first we choose D_k and U_k to start with. Then we find the best U_k with a quadratic descent method.[11] The next step is to try to improve D_k given the gradient

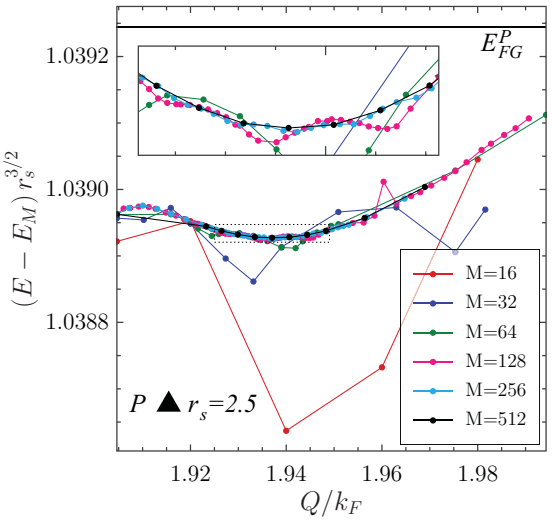

FIG. 3. (Color online) Variation of the energy of the 2DEG at $r_s = 2.5$ with triangular symmetry vs Q for different values of $N_{\mathcal{B}} = M^2$. The inset is the zoom of the region represented by the dashed rectangle.

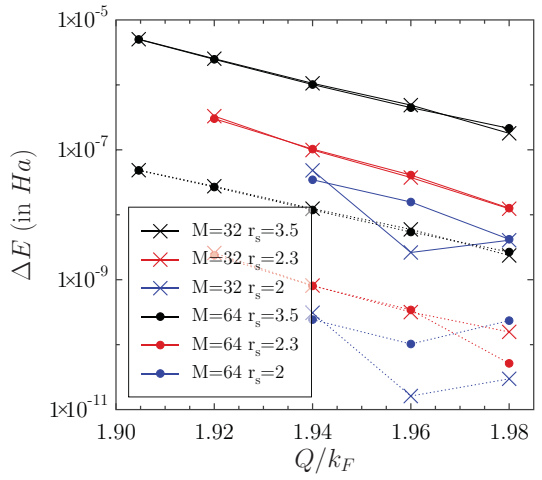

FIG. 4. (Color online) Convergence of the energy with respect to M_Λ for the 2DEG with triangular symmetry for two system sizes, $M = 32$ and $M = 64$. Solid and dotted lines indicate $\Delta E = E_{M_{\Lambda,1}} - E_{M_{\Lambda,2}}$ and $\Delta E = E_{M_{\Lambda,2}} - E_{M_{\Lambda,3}}$, respectively, with $M_{\Lambda,1} = 7$, $M_{\Lambda,2} = 13$, and $M_{\Lambda,3} = 19$. Crosses and dots stand for $M = 32$ and 64, respectively. (Values at $r_s = 2$ are close to the convergence threshold of the descent method.)

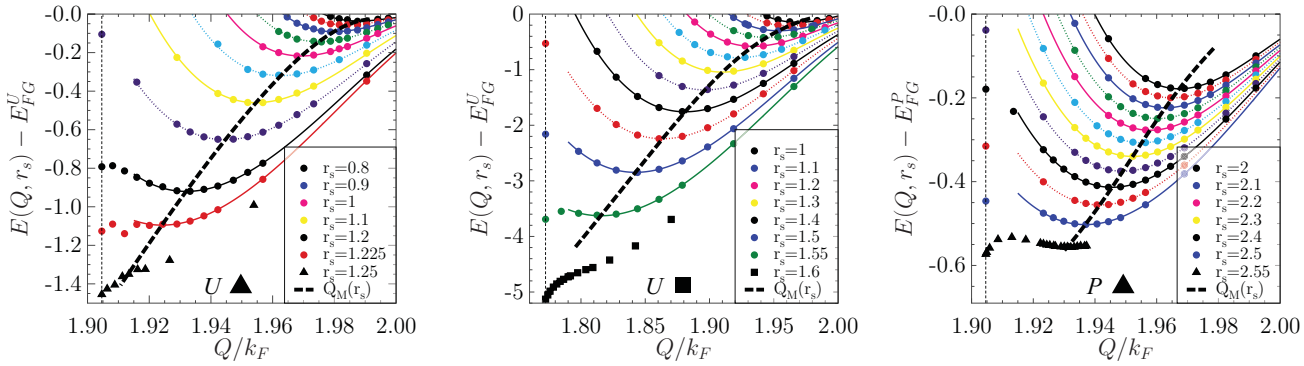

FIG. 5. (Color online) Energy difference, with respect to the Fermi gas, $E(Q,r_s) - E^{U/P}_{\rm FG}$, in milli-Hartree vs modulation Q for different densities and symmetries (triangular or square) at $N_{\mathcal{B}} = 256 \times 256$. The final polarization obtained after minimization is either unpolarized (U) or fully polarized (P). Lines are the polynomial fits using the parameters given in Table I. In each plot, the lowest curve (largest r_s) with triangular or square symbols has a minimum at $Q = Q_W$. The thick dashed line connects $Q_M(r_s)$, the minima of $E(Q,r_s)$ for fixed r_s. Vertical dotted lines indicate Q_W.

of the energy with respect to D_k and the linear constrains, $0 \leqslant D_k \leqslant 1/N$ and $\sum_k D_k = 1$. The process stops as soon as $D_k^{(\rm new)} = D_k$. In this case almost every D_k is 0 or $1/N$, and the gradient is negative or positive accordingly. Otherwise, we change D_k into $(1-\varepsilon)D_k + \varepsilon D_k^{(\rm new)}$ (with a small ε to ensure that U_k follows D_k *adiabatically*), and we restart the minimization with respect to U_k.

In this work, we study the 2DEG for triangular and square symmetries where $\|Q_1\| = \|Q_2\| = Q$. Starting from a state of arbitrary polarization, the minimization always resulted in either a U or a P state. The Brillouin zone of the Wigner crystal contains exactly N states, so that $Q/k_F = Q_W/k_F = \sqrt{2\pi/\sqrt{3}} \approx 1.9046$ for the triangular WC (U or P), whereas $Q/k_F = Q_W/k_F = \sqrt{\pi} \approx 1.7725$ for the square WC (U or P). Notice that for triangular symmetry the corresponding direct space lattices are quite different: a honeycomb lattice for unpolarized and a triangular lattice for polarized states. The FG can be reached when the Fermi surface is contained inside the Brillouin zone, that is, for $Q \geqslant 2k_F$. Thus, in our simulations, Q varies between Q_W and $2k_F$.

III. CONVERGENCE STUDIES

We first focus on size effects in the thermodynamic limit extrapolation, $N \to \infty$. We set $Q_i = ML_i^*$; thus the Brillouin zone contains $N_{\mathcal{B}} = M^2$ vectors. Since $N/N_{\mathcal{B}} = (Q_W/Q)^2$, this limit at fixed Q is equivalent to study the convergence with respect to $N_{\mathcal{B}}$. Figure 2 shows the size extrapolation of the 2DEG in the triangular symmetry at $r_s = 4$ ($Q = Q_W$), together with the results of Trail *et al.*,[15] done at $N_{\mathcal{B}} = 13$ and $M_\Lambda \simeq 20$, and those of Ref. 11. As the calculations of Ref. 11 do not assume any periodicity in the HF search, they are limited to system sizes $N \lesssim 500$, and the extrapolation to the thermodynamic limit is less accurate.

Size effects depend on the phase considered. In the incommensurate phase, size corrections are no longer monotonic functions, as in the Wigner crystal, but oscillatory behavior occurs depending on the density r_s and on the modulation vector Q. In Fig. 3, we show the energy of the 2DEG in a triangular symmetry at $r_s = 2.5$ versus the modulation Q (incommensurate crystal) for various system sizes using $M = 2^p$, with p from 4 to 9 ($N_{\mathcal{B}} = 16^2$ up to 512^2). Note the random-like oscillations due to the discretization $N_{\mathcal{B}}$ of the Brillouin zone. However, at large enough $N_{\mathcal{B}}$, these oscillations are sufficiently small to analyze safely $E(Q,r_s)$, as seen in Fig. 5.

Our second parameter is the number of vectors M_Λ considered in Λ. Note that truncation of Λ does not violate the variational principle, so that the energy of a converged HF solution must decrease as M_Λ increases. Figures 2 and 4 show the convergence in system size $N_{\mathcal{B}}$ (discretization of the Brillouin zone) together with the exponential convergence in M_Λ, which measures the large k importance. As expected, energies decrease with M_Λ because the Hilbert space is increased. Interestingly, the M_Λ improvement is mainly independent of $N_{\mathcal{B}}$ (see Fig. 2, right, and Fig. 4), which allows us to work with small M_Λ and estimate corrections using small systems. Most of the calculations presented in this paper are thus performed with $M_\Lambda = 7$ and $M_\Lambda = 9$ bands for supercells of triangular and square symmetry, respectively.

TABLE I. Coefficients α_{ij} of the polynomial fits $E(Q,r_s) - E_{\rm FG}(r_s)$ defined by Eq. (6).

U triangular			U square			P triangular		
−0.78611	1.88240	−1.13180	−0.621900	1.53040	−0.96941	0.15758	−0.08577	−0.011495
0.35614	−0.64435	0.34780	0.058858	−0.26652	0.27359	0.24875	−0.24028	0.070520
0.10624	−0.15804	0.05531	0.032321	−0.06425	0.02500	0.11155	−0.10668	0.024822
−0.00166	−0.00044	0.00081	−0.022986	0.02665	−0.00750	−0.00090	−0.00321	0.001310

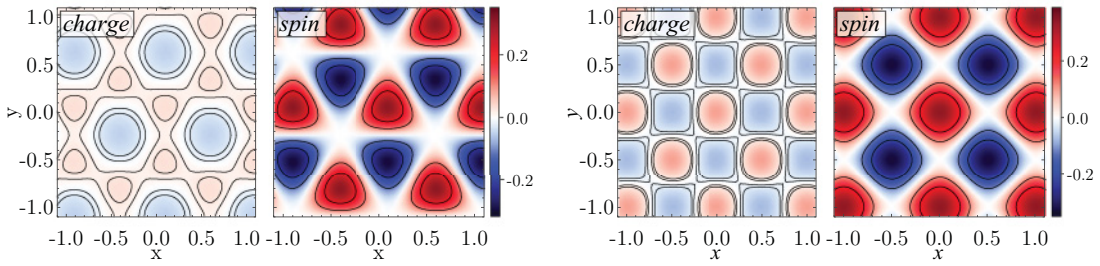

FIG. 6. (Color online) One-body charge and spin densities of an unpolarized incommensurate crystal with (left) triangular symmetry ($r_s = 1.2$, $Q/k_F = 1.933$, $N/N_{\mathcal{B}} \simeq 0.97$) and (right) square symmetry ($r_s = 1.5$, $Q/k_F = 1.844$, $N/N_{\mathcal{B}} \simeq 0.92$). Average values have been subtracted. Lengths are given in units of the inverse modulation Q^{-1}. The color scaling is the same for all pictures. Contour levels are at ± 0.01, ± 0.02 for the charge densities and at ± 0.1, ± 0.2 for the spin densities.

IV. RESULTS

We have studied the HF ground state of the 2DEG in the density region $0.8 \leqslant r_s \leqslant 4$ at zero temperature considering commensurate and incommensurate solutions with square and triangular symmetries. At low densities the electrons form a commensurate Wigner crystal of modulations $Q = Q_W$, and we recover the results of previous HF studies.[11,15,17] For higher densities, an incommensurate crystal with modulation $Q_W < Q < 2k_F$ is formed for any fixed polarization and symmetry.

Figure 5 summarizes the energy gain with respect to the unmodulated Fermi gas as a function of Q at different densities. Well inside the incommensurate phase ($Q > Q_W$), the energies can be well represented with a polynomial form:

$$E(Q,r_s) = E_{\mathrm{FG}}(r_s) + \sum_{i=0}^{3}\sum_{j=0}^{2} \alpha_{ij} X^i r_s^j, \qquad (6)$$

where $X = 100(Q/k_F - 2)$. The parameters α_{ij} determined by least-squares fits are given in Table I. From this parametrization, for fixed r_s, we determine the minimum $Q_M(r_s)$ of $E(Q,r_s)$, shown in Fig. 5.

The incommensurate phase is characterized by a crystal in direct space with slightly more lattice sites $N_{\mathcal{B}}$ than electrons N, increasing for larger modulation according to $N_{\mathcal{B}}/N = (Q/Q_W)^2$. Figure 6 shows typical charge and spin densities in the incommensurate phase for the triangular and square geometries. The two examples are chosen close to the transition to the *Wigner* crystallization. The amplitude of the modulation of the charge densities is about an order of magnitude smaller than that of the spin densities, an effect that is even more pronounced at higher density.

The momentum distribution n_k (N times the diagonal part of ρ_1) provides additional insight. In contrast to the step-function behavior at k_F of the Fermi gas, n_k is

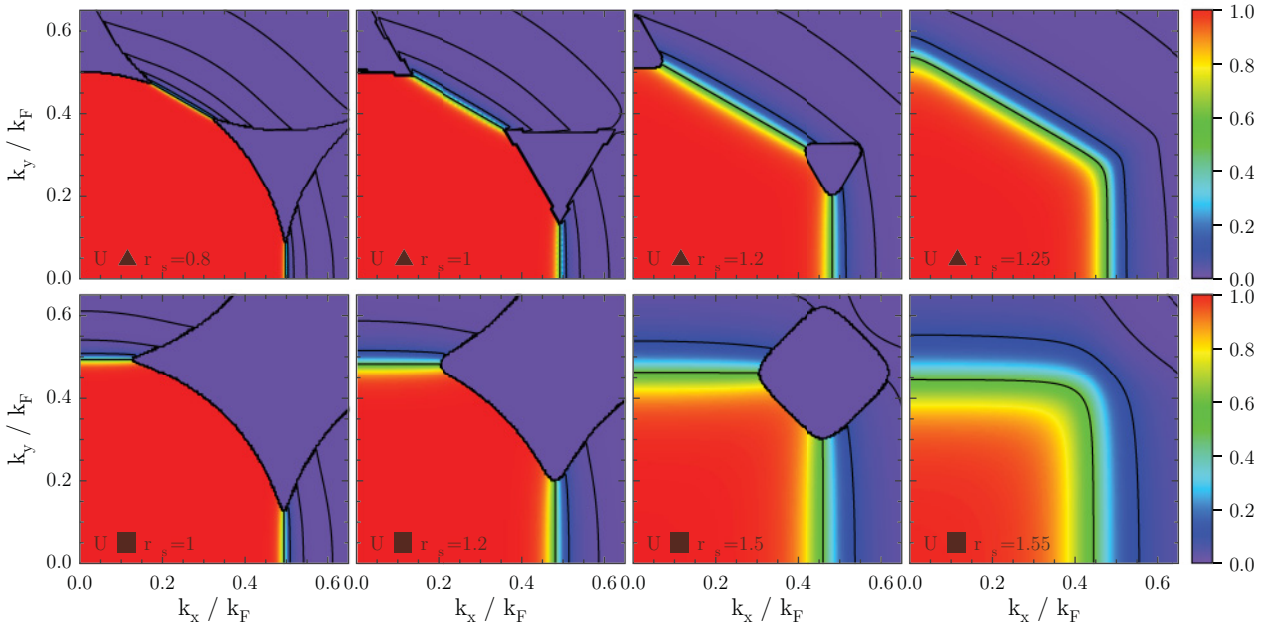

FIG. 7. (Color online) Modulus of the momentum distribution $|n_\uparrow(k)| = |n_\downarrow(k)|$ of U solutions as a function of wave vector k in the positive quadrant (other parts can be deduced by symmetry) for (top) triangular and (bottom) square symmetries. Contour levels are at 0.5 and 0.1, 0.01, etc. From right to left is shown the evolution from the Wigner-crystal distribution (continuous function everywhere) to the Fermi gas with a step along some directions. For the incommensurate states, note the step-function behavior to a domain where $n_k = 0$, which grows in the corner of the Brillouin zone when r_s decreases.

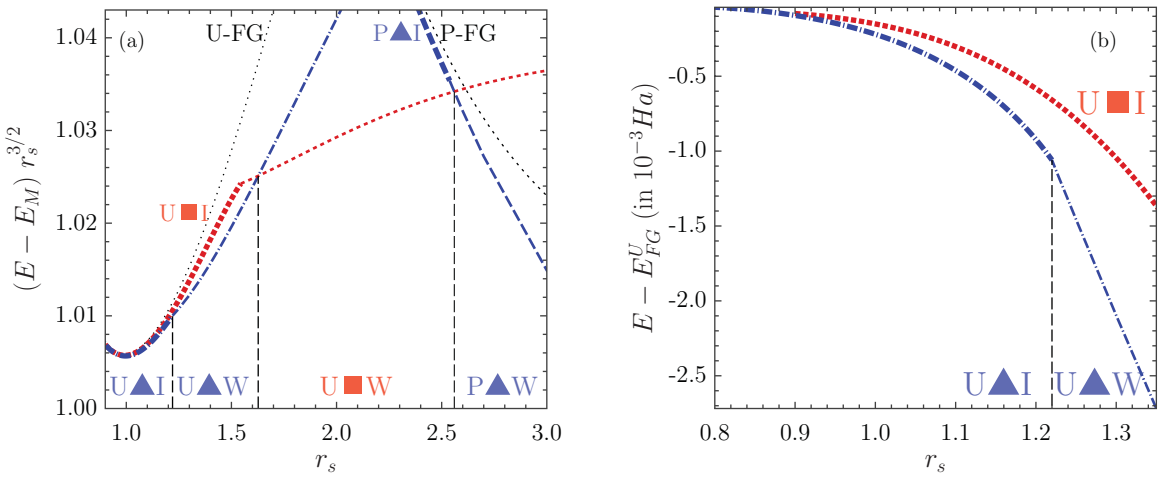

FIG. 8. (Color online) (a) Phase diagram of the 2DEG at $T = 0$, where $E_M = -1.1061/r_s$ is the Madelung energy and energies are multiplied by $r_s^{3/2}$. Dotted lines correspond to the Fermi gas. Blue and red curves represent the triangular and square phases, and P and U stand for polarized and unpolarized phases, respectively, whereas W and I (thick curves) indicate Wigner crystal and incommensurate crystal, respectively. The dashed vertical lines indicate the transitions. (b) Energy gain with respect to the unpolarized Fermi gas energy $E^U_{\rm FG}$ in the high-density region.

continuous inside the commensurate Wigner-crystal phase, and its variation reflects the symmetry of the Brillouin zone. The incommensurate phase still reflects the underlying symmetry of the crystal, but angle-selective steps occur at the corners of the Brillouin zone (see Fig. 7). The rounding of the corners increases for smaller r_s, and the isotropic step function of the Fermi gas is continuously approached for $r_s \to 0$.

Whereas we have found that the incommensurate phase is always favored compared to the Fermi gas solution, independently of the imposed polarization and crystal symmetry, the unpolarized incommensurate hexagonal crystal becomes the true HF ground state at high densities, $r_s \leqslant r_s^c \simeq 1.22$. The different phases and energies for $0.8 \leqslant r_s \leqslant 4.0$ are illustrated in Fig. 8. Although our HF method does not impose the polarization, we have not found any stable partially polarized ground states. At $r_s > r_s^c$ the unpolarized electrons form a commensurate Wigner crystal of hexagonal symmetry, and at $r_s \simeq 1.62$ a structural transition from the unpolarized hexagonal WC to the unpolarized square WC occurs, followed by a transition from the unpolarized square WC to the fully polarized triangular WC at $r_s \simeq 2.6$.

V. CONCLUSION

We have studied the 2DEG in the Hartree-Fock approximation at densities $r_s \lesssim 4$. We confirm previous observations of incommensurate phases of the fully polarized electron gas,[11] performing calculations of much larger system sizes. We further included electron polarization as well as square and triangular symmetries. Our HF phase diagram at zero temperature is much richer than that obtained previously,[15] which did not consider the unpolarized triangular WC or any incommensurate phase. Our numerical calculations explicitly confirm the old conjecture of Overhauser[9,10] that Fermi gas is never the HF ground state, which has been proven rigorously for the fully polarized electron gas.[11]

We have further shown that the momentum distribution provides an unambiguous characterization of the incommensurate phase. In contrast to the isotropic momentum distribution of a Fermi liquid, discontinuous at the Fermi surface,[18,19] the incommensurate phase exhibits an anisotropic momentum distribution intermediate between a crystal and the Fermi gas with forbidden domains inside the Brillouin zone, where n_k jumps to zero.

[1] S. Huotari, J. A. Soininen, T. Pylkkänen, K. Hämäläinen, A. Issolah, A. Titov, J. McMinis, J. Kim, K. Esler, D. M. Ceperley, M. Holzmann, and V. Olevano, Phys. Rev. Lett. **105**, 086403 (2010).
[2] B. Bernu, F. Delyon, and M. Holzmann, Phys. Rev. B **82**, 245116 (2010).
[3] T. Ando, A. B. Fowler, and F. Stern, Rev. Mod. Phys. **54**, 437 (1982).
[4] E. P. Wigner, Trans. Faraday Soc. **34**, 678 (1938); Phys. Rev. **46**, 1002 (1934).
[5] D. M. Ceperley and B. J. Alder, Phys. Rev. Lett. **45**, 566 (1980).
[6] B. Tanatar and D. M. Ceperley, Phys. Rev. B **39**, 5005 (1989).
[7] B. Bernu, L. Cândido, and D. M. Ceperley, Phys. Rev. Lett. **86**, 870 (2001).
[8] L. Cândido, B. Bernu, and D. M. Ceperley, Phys. Rev. B **70**, 094413 (2004).
[9] A. W. Overhauser, Phys. Rev. Lett. **4**, 462 (1960); Phys. Rev. **128**, 1437 (1962).
[10] G. F. Giuliani and G. Vignale, *Quantum Theory of the Electron Liquid* (Cambridge University Press, Cambridge, 2005).

[11]B. Bernu, F. Delyon, M. Duneau, and M. Holzmann, Phys. Rev. B **78**, 245110 (2008).
[12]B. Spivak and S. A. Kivelson, Phys. Rev. B **70**, 155114 (2004).
[13]B. K. Clark, M. Casula, and D. M. Ceperley, Phys. Rev. Lett. **103**, 055701 (2009).
[14]H. Falakshahi and X. Waintal, Phys. Rev. Lett. **94**, 046801 (2005); X. Waintal, Phys. Rev. B **73**, 075417 (2006).
[15]J. R. Trail, M. D. Towler, and R. J. Needs, Phys. Rev. B **68**, 045107 (2003).
[16]S. Zhang and D. M. Ceperley, Phys. Rev. Lett. **100**, 236404 (2008).
[17]Using the same parameters, we recover exactly the results of Trail *et al*.[15] for the 2DEG (P triangular) at $r_s > 3$. We thank the authors for sending us their data.
[18]M. Holzmann, B. Bernu, V. Olevano, R. M. Martin, and D. M. Ceperley, Phys. Rev. B **79**, 041308 (2009).
[19]M. Holzmann, B. Bernu, C. Pierleoni, J. McMinis, D. M. Ceperley, V. Olevano, and L. Delle Site, Phys. Rev. Lett. **107**, 110402 (2011).